minerals

MDPI

Article

Extraction of Boron from Ludwigite Ore: Mechanism of Soda-Ash Roasting of Lizardite and Szaibelyite

Xin Zhang, Guanghui Li, Jinxiang You, Jian Wang, Jun Luo, Jiaoyang Duan, Tao Zhang, Zhiwei Peng, Mingjun Rao * and Tao Jiang

School of Minerals Processing and Bioengineering, Central South University, Changsha 410083, China
* Correspondence: mj.rao@csu.edu.cn; Tel.: +86-731-8883-0542

Received: 30 July 2019; Accepted: 30 August 2019; Published: 31 August 2019



Abstract: Ludwigite ore is a typical low-grade boron ore accounting for 58.5% boron resource of China, which is mainly composed of magnetite, lizardite and szaibelyite. During soda-ash roasting of ludwigite ore, the presence of lizardite hinders the selective activation of boron. In this work, lizardite and szaibelyite were prepared and their soda-ash roasting behaviors were investigated using thermogravimetric-differential scanning calorimetry (TG-DSC), X-ray diffraction (XRD), and scanning electron microscope and energy dispersive spectrometer (SEM-EDS) analyses, in order to shed light on the soda-ash activation of boron within ludwigite ore. Thermodynamics of Na_2CO_3-$MgSiO_3$-Mg_2SiO_4-$Mg_2B_2O_5$ via FactSage show that the formation of Na_2MgSiO_4 was preferential for the reaction between Na_2CO_3 and $MgSiO_3$/Mg_2SiO_4. While, regarding the reaction between Na_2CO_3 and $Mg_2B_2O_5$, the formation of $NaBO_2$ was foremost. Raising temperature was beneficial for the soda-ash roasting of lizardite and szaibelyite. At a temperature lower than the melting of sodium carbonate (851 °C), the soda-ash roasting of szaibelyite was faster than that of lizardite. Moreover, the melting of sodium carbonate accelerated the reaction between lizardite with sodium carbonate.

Keywords: boron; ludwigite; soda ash roasting; szaibelyite; lizardite

1. Introduction

Boron is widely used in glass, ceramic, abstergent and fertilizers, accounting for three-quarters of the global boron consumption annually, in which borax and boric acid are the most commonly traded commodities [1]. Boron reserves in China are mainly ludwigite ore, which accounts for 58.5% boron resource [2]. Nevertheless, the average content of B_2O_3 is merely 7 wt.%, which is far lower than those of Turkey, USA, etc. [3,4]. As the increasing demand for boron resource, the effective utilization of the ludwigite ore is imperative to supply boron for China domestically.

Ludwigite ore reserved in China (mainly in Liaoning and Jilin Provinces) is a typical low-grade boron ore, which is mainly composed of magnetite (Fe_3O_4), lizardite ($Mg_3Si_2O_5(OH)_4$) and szaibelyite ($Mg_2B_2O_4(OH)_2$) [5,6]. It has yet to be utilized on a large scale, due to its low B_2O_3 grade and the complex mineralogy [7,8]. Extensive efforts have been paid to recover boron, as well as other valuable components [9–12]. The soda-ash roasting method has been proved to be an effective way for boron extraction from low-grade ludwigite ore, by improving the leaching activity of B_2O_3 with the aid of sodium carbonate [13,14]. Recently, an alternative method for simultaneously recovering boron and iron has been proposed in our previous research, with the advantage of low-cost synthesis of sodium metaborate ($NaBO_2{\cdot}2H_2O$) and preparation of powdery DRI (direct reduction iron) [15]. The simultaneous boron activation, along with iron metallization in a reductive atmosphere enables the comprehensive utilization of valuable components from ludwigite ore. This process simplifies the subsequent separating and synthesizing procedures, compared to many other trials, such as smelting

reduction followed by alkali leaching in order to recover iron and boron stepwise [9,11], and molten sodium hydroxide leaching to utilize boron individually [16–18].

During soda-ash roasting of ludwigite ore, sodium carbonate would react with both szaibelyite and lizardite, hindering the selective activation of boron. Hence, the dosage of sodium carbonate and the roasting conditions were closely relevant to the soda-ash roasting of ludwigite ore in the roasting process. In this work, lizardite and szaibelyite were prepared, and their behaviors of soda-ash roasting were investigated, in order to shed light on the soda-ash activation of boron within ludwigite ore.

2. Materials and Methods

2.1. Materials

Lizardite and szaibelyite were prepared from natural ores. The as-prepared samples were dried, crushed, ground and screened to 80% passing through 0.074 mm. Chemical composition and XRD patterns of these two samples are given in Table 1 and Figure 1, respectively. The corresponding purities of lizardite (calculated by SiO_2 content in the form of $Mg_3Si_2O_5(OH)_4$) and szaibelyite (calculated by B_2O_3 content in the form of $Mg_2B_2O_5{\cdot}H_2O$) are 86.3% and 94.6%, respectively.

Table 1. Main chemical composition of as-prepared lizardite and szaibelyite (wt.%).

Samples	TFe	B_2O_3	SiO_2	CaO	MgO	K_2O
Lizardite	5.50	ND*	37.36	1.24	41.82	0.04
Szaibelyite	1.87	39.16	0.74	0.88	46.21	0.15

ND*: Not detected.

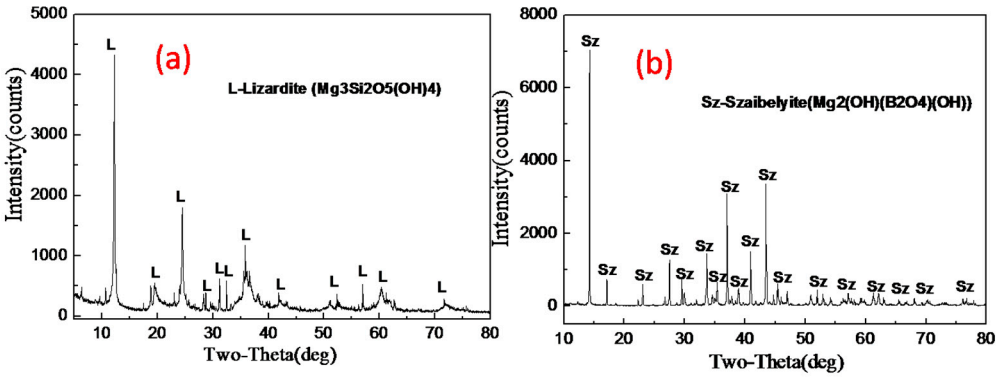


Figure 1. XRD patterns of as-prepared (**a**) lizardite and (**b**) szaibelyite samples.

To identify the dehydroxylation products, lizardite and szaibelyite were roasted at 1000 °C for 60 min in a nitrogen atmosphere, and their XRD patterns are presented in Figure 2. Forsterite (Mg_2SiO_4) and enstatite ($MgSiO_3$) were formed after dihydroxylation of lizardite, while suanite ($Mg_2B_2O_5$) was the main component of dihydroxylation of szaibelyite.

Nitrogen gas with high purity (99.999%) and sodium carbonate of analytical reagent (AR) grade were purchased and used in this work.

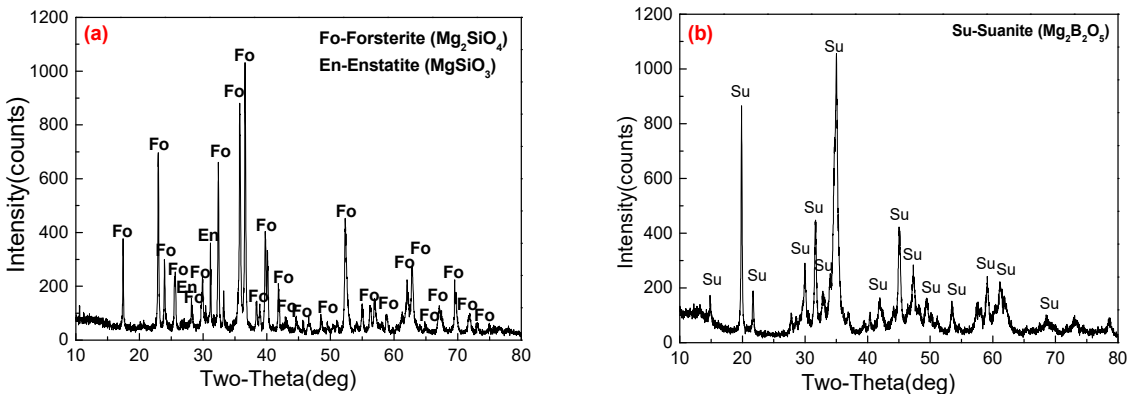


Figure 2. XRD results of the roasting products of lizardite (**a**) and szaibelyite (**b**).

2.2. Soda-Ash Roasting

The ground samples of lizardite and szaibelyite were thoroughly mixed with sodium carbonate chemical reagent with the molar ratio of 1:2 and 1:1, respectively. Every two-gram mixture was briquetted into a cylinder with 10 mm in diameter under the pressure of 10 MPa. The green cylinders were dried at 110 °C for 2 h. Subsequently, the dried cylinders were placed in a porcelain crucible and loaded into a quartz tube (the inner diameter of the quartz tube of 20 mm). The samples were pushed to the roasting zone in an electrically heated horizontal tube furnace. Before-hand, the furnace was heated to a preset temperature. The roasting temperature was measured with a Pt-Rh thermocouple and controlled using a KSY intelligent temperature controller (±5 °C). The experimental schematic diagram is described in Figure 3. High-purity of nitrogen gas (99.999%) was introduced to the quartz tube throughout the roasting process, and the gas flow rate was fixed at 200 L/h. After roasting, the briquettes were taken out of the furnace for cooling to room temperature in air atmosphere.

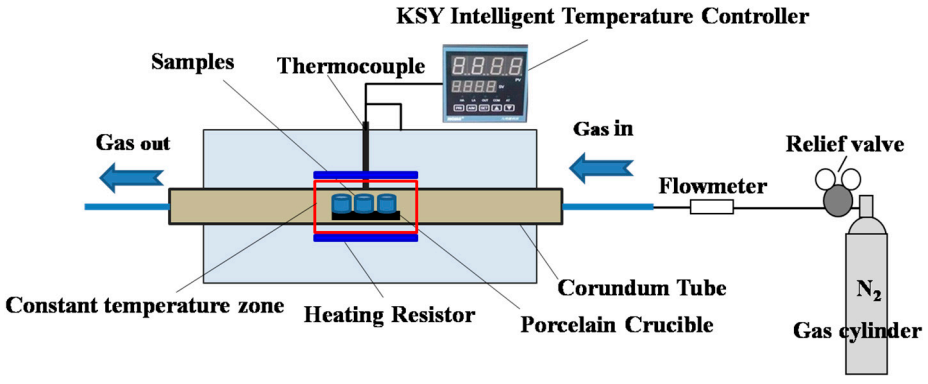


Figure 3. Schematic diagram of the equipment for soda-ash roasting.

2.3. Characterization

The chemical compositions of lizardite and szaibelyite samples were determined using an inductively coupled plasma atomic emission spectrometer (ICP-AES, ICAP-7600, Thermo Fisher Scientific, Waltham, MA, USA). Mineral components of roasted briquettes were analyzed by XRD (RIGAKU D/Max 2500, Tokyo, Japan) using Cu Kα radiation (k = 0.154178 nm) with 40 kV scanning voltage and 40 mA scanning current ranging from 10° to 80°. Thermogravimetric-differential scanning calorimetry (TG-DSC) tests were conducted in a simultaneous thermal analyzer (Netzsch STA 449F3, Düsseldorf, Germany). Meanwhile, a part of roasted briquettes was fixed into an epoxy resin mould, ground and polished to prepare cross-sections for SEM-EDS (TESCAN MIRA3, Brno, Czech Republic) analysis.

3. Results and Discussion

3.1. Thermodynamic Analysis

To identify the reaction priority of lizardite and szaibelyite with sodium carbonate, standard Gibbs free energies of related reactions were calculated using software FactSage 7.1. Considering the dehydroxylation of lizardite and szaibelyite during roasting, the related reactions and the corresponding standard Gibbs free energies of Na_2CO_3-$MgSiO_3$/Mg_2SiO_4 and Na_2CO_3-$Mg_2B_2O_5$ systems were calculated.

3.1.1. Na_2CO_3-$MgSiO_3$/Mg_2SiO_4 System

Table 2 shows the possible reactions of Na_2CO_3-$MgSiO_3$ and Na_2CO_3-Mg_2SiO_4 systems. The relationship between Gibbs free energy and temperature was plotted in Figure 4.

Table 2. ΔrG_m^{Θ} − T equations of Na_2CO_3-MgO-SiO_2 system during roasting (400 °C < T < 1400 °C).

Reaction	Equation	ΔrG_m^{Θ} − T (kJ·mol^{-1})
(1)	$2/3MgSiO_3 + Na_2CO_3 = 1/3Na_6Si_2O_7 + 2/3MgO + CO_2(g)$	76.46 − 0.10T
(2)	$MgSiO_3 + Na_2CO_3 = Na_2SiO_3 + MgO + CO_2(g)$	53.69 − 0.09T
(3)	$2MgSiO_3 + Na_2CO_3 = Na_2Si_2O_5 + 2MgO + CO_2(g)$	90.08 − 0.12T
(4)	$1/2MgSiO_3 + Na_2CO_3 = 1/2Na_4SiO_4 + 1/2MgO + CO_2(g)$	82.59 − 0.09T
(5)	$1/5MgSiO_3 + Na_2CO_3 = 1/5Na_{10}SiO_7 + 1/5MgO + CO_2(g)$	213.66 − 0.13T
(6)	$8/3MgSiO_3 + Na_2CO_3 = 1/3Na_6Si_8O_{19} + 8/3MgO + CO_2(g)$	109.95 − 0.12T
(7)	$6MgSiO_3 + Na_2CO_3 = Na_2Mg_2Si_6O_{15} + 4MgO + CO_2(g)$	193.07 − 0.20T
(8)	$4MgSiO_3 + Na_2CO_3 = Na_2MgSi_4O_{10} + 3MgO + CO_2(g)$	139.01 − 0.16T
(9)	$MgSiO_3 + Na_2CO_3 = Na_2MgSiO_4 + CO_2(g)$	99.06 − 0.14T
(10)	$2/3Mg_2SiO_4 + Na_2CO_3 = 1/3Na_6Si_2O_7 + 4/3MgO + CO_2(g)$	103.42 − 0.11T
(11)	$Mg_2SiO_4 + Na_2CO_3 = Na_2SiO_3 + 2MgO + CO_2(g)$	85.62 − 0.10T
(12)	$2Mg_2SiO_4 + Na_2CO_3 = Na_2Si_2O_5 + 4MgO + CO_2(g)$	153.93 − 0.13T
(13)	$1/2Mg_2SiO_4 + Na_2CO_3 = 1/2Na_4SiO_4 + MgO + CO_2(g)$	98.09 − 0.09T
(14)	$1/5Mg_2SiO_4 + Na_2CO_3 = 1/5Na_{10}SiO_7 + 2/5MgO + CO_2(g)$	219.61 − 0.13T
(15)	$8/3Mg_2SiO_4 + Na_2CO_3 = 1/3Na_6Si_8O_{19} + 16/3MgO + CO_2(g)$	194.65 − 0.13T
(16)	$6Mg_2SiO_4 + Na_2CO_3 = Na_2Mg_2Si_6O_{15} + 10MgO + CO_2(g)$	384.16 − 0.22T
(17)	$4Mg_2SiO_4 + Na_2CO_3 = Na_2MgSi_4O_{10} + 7MgO + CO_2(g)$	266.27 − 0.18T
(18)	$Mg_2SiO_4 + Na_2CO_3 = Na_2MgSiO_4 + MgO + CO_2(g)$	128.39 − 0.15T

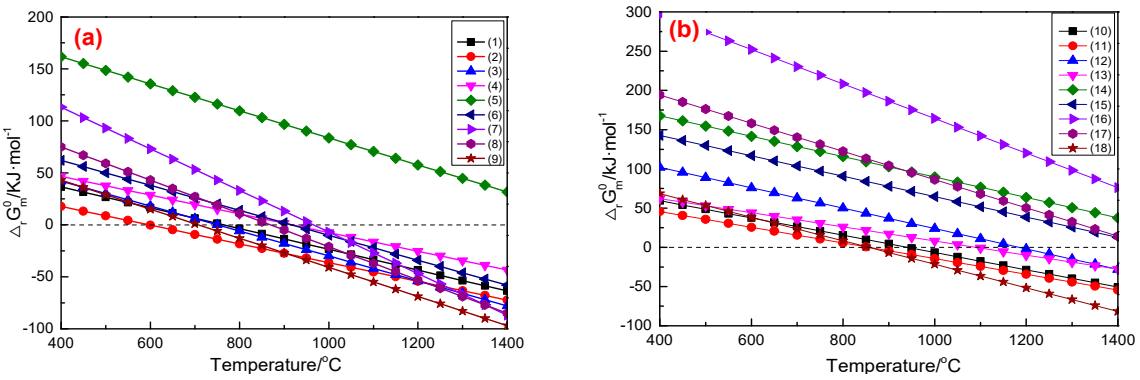


Figure 4. Plots of Gibbs free energy against the temperature of (**a**) Na_2CO_3-$MgSiO_3$ and (**b**) Na_2CO_3-Mg_2SiO_4.

It can be seen from Figure 4a that the Gibbs free energy of Reactions (1–4) and (6–9) kept negative in the temperature range 400–1400 °C, indicating the reactions of $MgSiO_3$ and Na_2CO_3 into a variety of sodium silicates or sodium magnesium silicates were thermodynamically favorable. The starting reaction temperatures of each reaction are 764.60 °C, 596.56 °C, 750.67 °C, 917.67 °C, 916.25 °C, 965.35 °C, 868.81 °C and 707.57 °C, respectively. When the temperature was below 907.40 °C, the generation of

Na_2SiO_3 was preferential, while the generation of Na_2MgSiO_4 was the first priority as the temperature exceeded 907.40 °C. Meanwhile, the Gibbs free energy of Reaction (5) kept positive, which signified the generation of $Na_{10}SiO_7$ was thermodynamically unfavorable in the temperature range 400–1400 °C.

Likewise, it can be seen from Figure 4b that the Gibbs free energy of Reactions (14–17) kept positive, while the others kept negative at the carbon dioxide pressure of 1atm, indicating that the reactions of M_2gSiO_4 and Na_2CO_3 into $Na_{10}SiO_7$, $Na_6Si_8O_{19}$, $Na_2Mg_2Si_6O_{15}$ and $Na_2MgSi_4O_{10}$ were thermodynamically infeasible. The starting formation temperatures of $Na_6Si_2O_7$, Na_2SiO_3, $Na_2Si_2O_5$, Na_4SiO_4, Na_2MgSiO_4 are 940.18 °C, 856.20 °C, 1184.08 °C, 1089.89 °C, 855.93 °C, respectively.

Thus, for the reaction between sodium carbonate, $MgSiO_3$ and Mg_2SiO_4, the generation of Na_2MgSiO_4 was preferential in the temperature range 400–1400 °C, and the starting reaction temperatures are 707.57 °C and 855.93 °C, respectively.

3.1.2. Na_2CO_3-$Mg_2B_2O_5$ System

Table 3 shows the reactions of Na_2CO_3-$Mg_2B_2O_5$ system and their corresponding standard Gibbs free energies. The relationship between Gibbs free energy and temperature was plotted in Figure 5. The results demonstrated that the formation of $NaBO_2$, $Na_4B_2O_5$ and Na_3BO_3 are feasible. Among these three products, the formation of $NaBO_2$ was preferential, and the starting reaction temperature was 1000 °C.

Table 3. ΔrG_m^{Θ} − T equations of Na_2CO_3-$Mg_2B_2O_5$ system during roasting (400 °C < T < 1400 °C).

Reaction	Equation	ΔrG_m^{Θ} − T (kJ·mol^{-1})
(19)	$Mg_2B_2O_5 + Na_2CO_3 = 2NaBO_2 + 2MgO + CO_2(g)$	130.16 − 0.13T
(20)	$1/3Mg_2B_2O_5 + Na_2CO_3 = 2/3Na_3BO_3 + 2/3MgO + CO_2(g)$	133.03 − 0.10T
(21)	$1/2Mg_2B_2O_5 + Na_2CO_3 = 1/2Na_4B_2O_5 + MgO + CO_2(g)$	145.77 − 0.14T
(22)	$2Mg_2B_2O_5 + Na_2CO_3 = Na_2B_4O_7 + 4MgO + CO_2(g)$	174.42 − 0.07T
(23)	$3Mg_2B_2O_5 + Na_2CO_3 = 2NaB_3O_5 + 6MgO + CO_2(g)$	256.21 − 0.05T

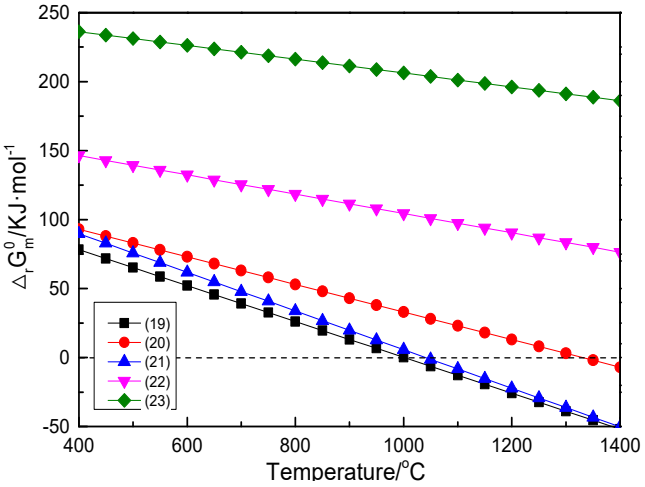


Figure 5. Plots of Gibbs free energy against the temperature of Na_2CO_3-$Mg_2B_2O_5$.

3.2. TG-DSC Analysis

3.2.1. Lizardite with Soda Ash

TG-DSC curves of lizardite, sodium carbonate and their mixture (molar ratio of lizardite to sodium carbonate 1:2) are shown in Figure 6.

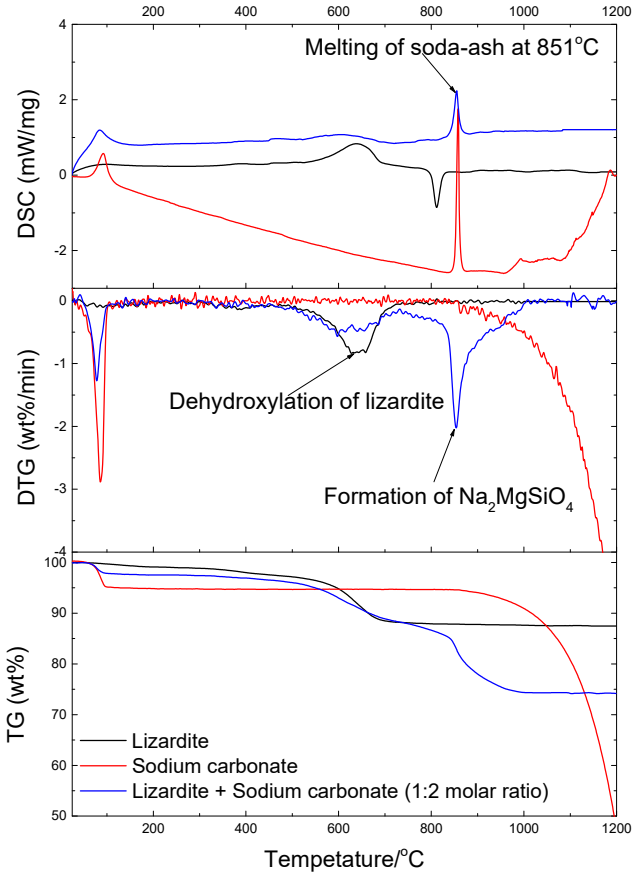


Figure 6. Thermogravimetric-differential scanning calorimetry (TG-DSC) curves of lizardite, sodium carbonate and the mixture of lizardite and sodium carbonate (argon atmosphere, 10 °C/min).

For sodium carbonate, a mass loss occurred around 78.1 °C was owing to the dehydration of crystallization water. The thermal decomposition of sodium carbonate started from its melting point at 851 °C [19].

For lizardite, firstly, an endothermic peak appeared at 639.5 °C with the mass loss of 13.1%. This was due to the dehydroxylation of lizardite whose mass loss was 13.0% theoretically according to Equation (24). Along with the increase of temperature, an exothermic peak appeared at 811.5 °C in the DSC curves without mass loss, which was attributed to the recrystallization of forsterite [20],

$$Mg_3Si_2O_5(OH)_4 = Mg_2SiO_4 + MgSiO_3 + 2H_2O. \quad (24)$$

The mixture of lizardite and sodium carbonate began to lose its weight at around 60 °C and came to an end at around 1000 °C, and the total mass loss was 25.8%. Based on the molar ratio of lizardite and sodium carbonate, the theoretical total mass loss should be 25.4% according to Equation (25),

$$Mg_3Si_2O_5(OH)_4 + 2Na_2CO_3 = 2Na_2MgSiO_4 + 2CO_2 + 2H_2O + MgO. \quad (25)$$

There were three distinct mass loss peaks (78.1 °C, 639.5 °C, 851 °C) in the DTG curve during the roasting process. As the temperature increased, a rapid mass loss of 13.9% took place. This resulted from the reaction between sodium carbonate and the dehydroxylation product of lizardite, as shown in Table 2. The peak temperature of the DSC curve was 851 °C, which is the same with a melting point of sodium carbonate, illustrating that the melting of sodium carbonate accelerated this reaction.

3.2.2. Szaibelyite with Soda Ash

TG-DSC curves of szaibelyite, sodium carbonate and their mixture (molar ratio of szaibelyite to sodium carbonate is 1:1) are shown in Figure 7.

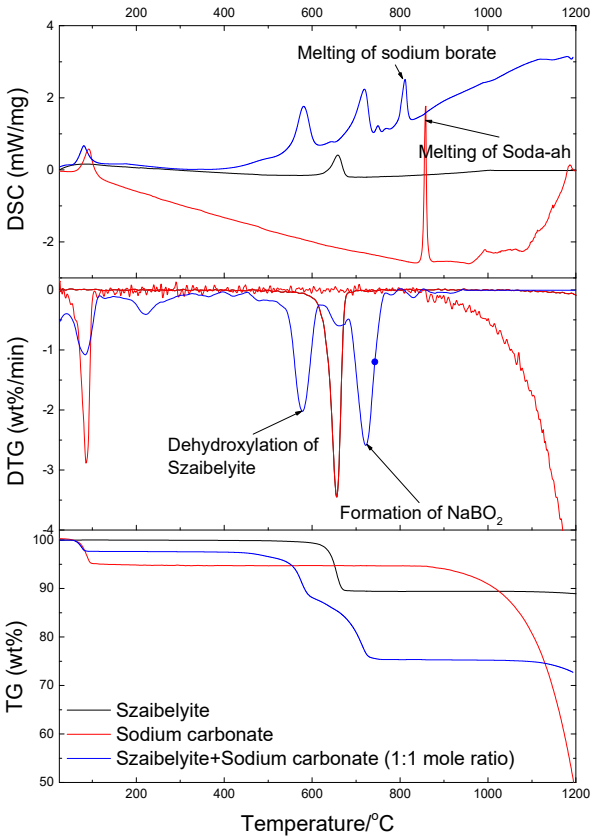


Figure 7. TG-DSC curves of szaibelyite, sodium carbonate and the mixture of szaibelyite and sodium carbonate (argon atmosphere, 10 °C/min).

For szaibelyite, there was an endothermic peak appeared at 659 °C in the DSC curve with mass loss of 10.4%. This was due to the dehydroxylation of szaibelyite, whose mass loss was 10.7% according to Equation (26),

$$Mg_2B_2O_4(OH)_2 = Mg_2B_2O_5 + H_2O. \quad (26)$$

The mixture began to lose mass from around 80 °C until the temperature increased to around 760 °C. The total mass loss was 22.5%, while the theoretical mass loss was 22.6% according to Equation (27),

$$Mg_2B_2O_4(OH)_2 + Na_2CO_3 = 2NaBO_2 + CO_2 + H_2O + 2MgO. \quad (27)$$

There were three obvious mass loss peaks (80.72 °C, 580.20 °C, 718.55 °C) in the DTG curve during the roasting process, with corresponding three endothermic peaks in the DSC curve. The mass loss peak of 7.2% at 580.20 °C was mainly due to the dehydroxylation of szaibelyite, whose theoretical mass loss was 6.4%. Compared to the DSC curve of pure szaibelyite, the dehydroxylation of szaibelyite was advanced when sodium carbonate was added.

Furthermore, a mass loss peak appeared at 718.55 °C with the mass loss of 15.1% was attributed to the reactions between the dehydroxylation products of szaibelyite and sodium carbonate, as shown in Table 3. It was worth noting that an endothermic peak at 851 °C disappeared in the DSC curve of the mixture, indicating that sodium carbonate had been completely consumed before its melting point.

3.3. Phase Transformation and Microstructure

3.3.1. Effect of Roasting Temperature

The mixtures of sodium carbonate with lizardite or szaibelyite were both roasted for 60 min in a nitrogen atmosphere at different temperatures. The molar ratio of lizardite to sodium carbonate was 1:2, while the molar ratio of szaibelyite to sodium carbonate was 1:1, and the corresponding XRD patterns are displayed in Figure 8.

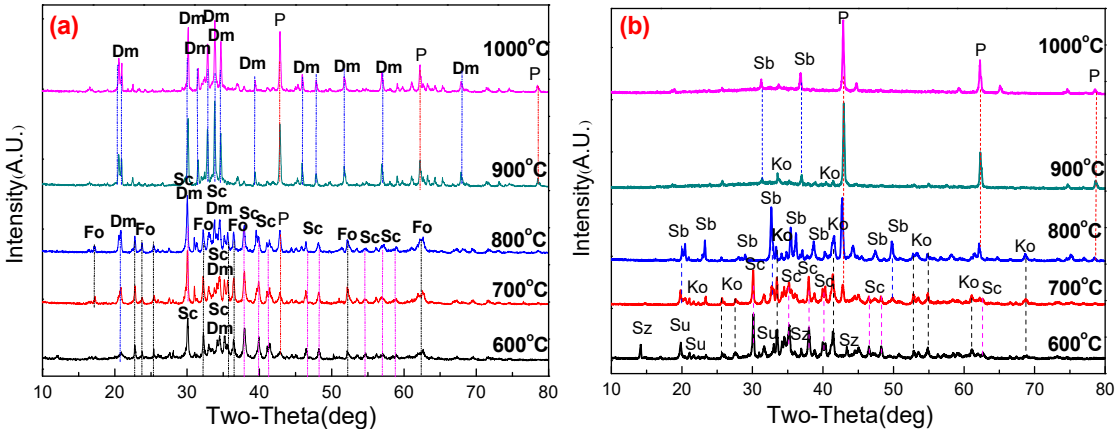


Figure 8. XRD patterns of (**a**) mixture of lizardite and sodium carbonate (lizardite to sodium carbonate molar ratio 1:2) and (**b**) mixture of szaibelyite and carbonate (szaibelyite to sodium carbonate molar ratio 1:1) at different temperatures for 60 min in a nitrogen atmosphere. Sc—Sodium carbonate (Na_2CO_3); Fo—Forsterite (Mg_2SiO_4); Dm—Disodium magnesiosilicate (Na_2MgSiO_4); P—Periclase (MgO); Sz—szaibelyite ($Mg_2B_2O_4(OH)_2$); Su—suanite ($Mg_2B_2O_5$); Ko—kotoite ($Mg_3B_2O_6$); Sb—Sodium borate.

The roasting temperature had a significant impact on the soda-ash roasting behavior of lizardite and szaibelyite. In Figure 8a, the main phases of the roasted sample at 600 °C were sodium carbonate and forsterite from the dehydroxylation of lizardite, and limited content of disodium magnesiosilicate (Na_2MgSiO_4) and periclase (MgO). The diffraction peaks of sodium carbonate and forsterite weakened and disappeared when the roasting temperature above 900 °C, along with the strengthening of the diffraction peaks of Na_2MgSiO_4 and MgO. The generation of a large amount of Na_2MgSiO_4 and MgO further demonstrated that the kinetics of the solid-state reaction between sodium carbonate and forsterite is slow, while the melting of sodium carbonate accelerated this reaction.

XRD patterns of the mixture of szaibelyite and sodium carbonate roasted at different temperatures for 60 min are shown in Figure 8b. The phase components of the roasting product at 600 °C were szaibelyite, sodium carbonate, suanite and kotoite. As the roasting temperature increased, the phases of szaibelyite and suanite disappeared, along with the appearance of the new phases of periclase and sodium borate. The disappearance of szaibelyite was owing to its dehydroxylation, leading to the formation of suanite. The new-born suanite would react with sodium carbonate to form sodium borate, according to the reactions shown in Table 3. The diffraction peaks of sodium carbonate disappeared when the roasting temperature was above 800 °C, along with the strengthened diffraction peaks of sodium borate and periclase. This phenomenon further illustrated that sodium carbonate had completely reacted with the dehydroxylation products of szaibelyite before its melting point, which was in accordance with the TG-DSC results described above. The diffraction peaks no longer changed obviously when the roasting temperature increased to 1000 °C.

Hence, raising roasting temperature was beneficial for soda-ash roasting of lizardite and szaibelyite. At a temperature lower than the melting of sodium carbonate (851 °C), the soda-ash roasting kinetics of szaibelyite was faster than that of lizardite. The melting of sodium carbonate accelerated the reaction between lizardite with sodium carbonate.

3.3.2. Effect of Roasting Time

The effect of roasting time (5 min, 15 min, 30 min, 45 min and 60 min) on the reactions of mixtures of sodium carbonate with lizardite or szaibelyite is shown in Figure 9. The experiments were performed at 1000 °C in nitrogen atmosphere, and the molar ratio of lizardite to sodium carbonate was 1:1, while the molar ratio of szaibelyite to sodium carbonate was 1:2.

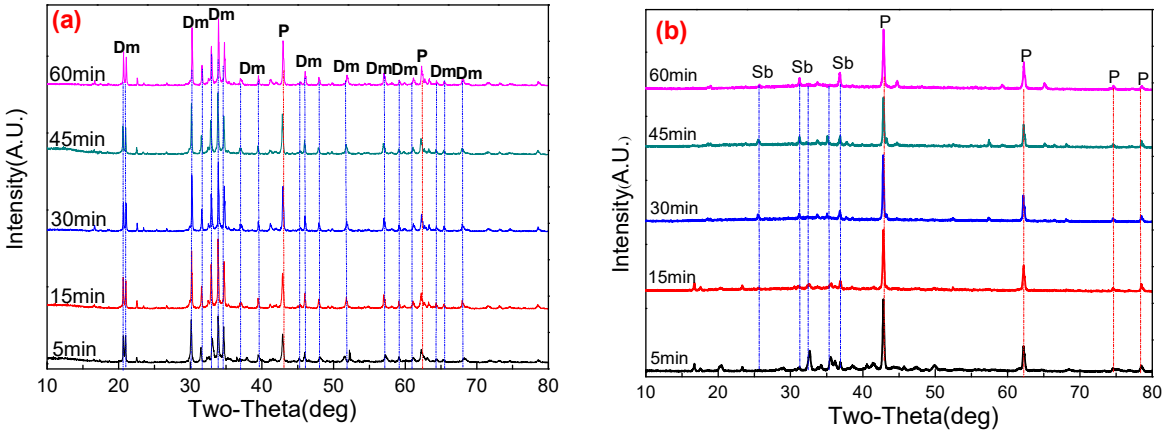
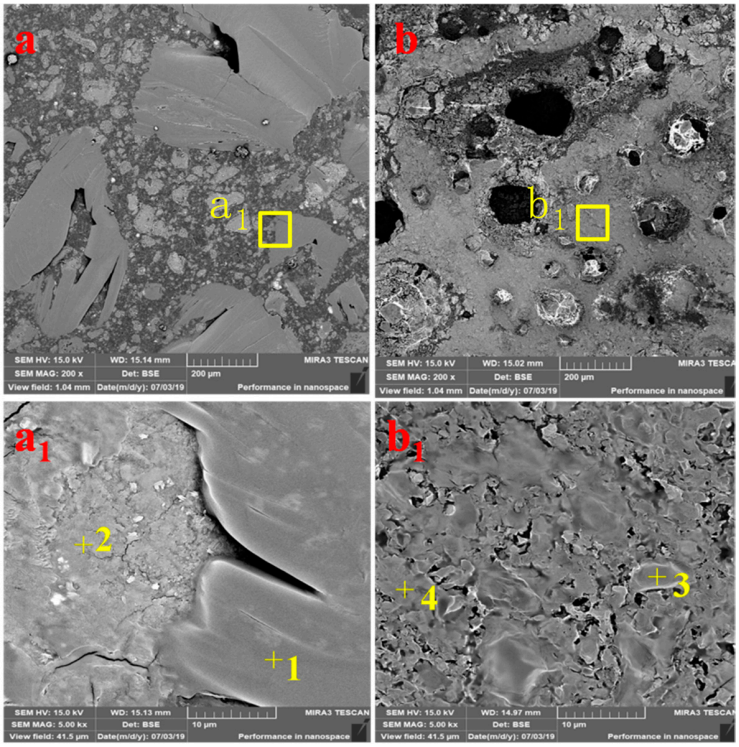


Figure 9. XRD patterns (**a**) mixture of lizardite and sodium carbonate (lizardite to sodium carbonate molar ratio 1:2) and (**b**) mixture of szaibelyite and carbonate (szaibelyite to sodium carbonate molar ratio 1:1) roasted at 1000 °C for a different time in nitrogen atmosphere. Dm—Disodium magnesiosilicate (Na_2MgSiO_4); P—Periclase (MgO); Sb—Sodium borate.

Roasting time had no obvious influence on the phase composition of the roasted samples in these two systems. For the XRD patterns in Figure 9, the diffraction peaks of Na_2MgSiO_4 and MgO appeared obviously when the roasting time was only 5 min. Similarly, the diffraction peaks of szaibelyite and sodium carbonate disappeared completely in such a short roasting time. Therefore, the reaction between sodium carbonate and lizardite/szaibelyite were extremely fast when the roasting temperature up to 1000 °C.

3.3.3. Microstructure

SEM images and corresponding EDS results of the mixtures both roasted at 800 °C for 60 min are shown in Figure 10. The main crystalline phases of the roasted mixture of lizardite and sodium carbonate were sodium carbonate (#1) and forsterite (#2), while the main phase of the roasted mixture of szaibelyite and sodium carbonate was sodium borates (#3, #4). The results further illustrated that, at the roasting temperature of 800 °C, lizardite partially reacted with sodium carbonate while szaibelyite reacted with sodium carbonate almost thoroughly, which agreed well with the phase transformation results.



Elements/ atom%	#1	#2	#3	#4
Na	34.15	2.74	10.57	15.02
B	ND*	ND*	36.43	29.56
Si	4.37	19.91	0.04	ND*
Mg	0.12	26.51	0.35	ND*
C	15.26	ND	ND	ND*
O	46.1	50.84	53	55.42

ND*: Not detected

Figure 10. SEM-EDS results of (**a**) mixture of lizardite and sodium carbonate with molar ratio of 1:2 and, (**b**) mixture of szaibelyite and sodium carbonate with molar ratio of 1:1, roasted at 800 °C for 60 min in a nitrogen atmosphere. a1 and b1 are the partial enlarged details corresponding to a and b, respectively.

4. Conclusions

In this work, lizardite and szaibelyite were prepared, and their behaviors of soda-ash roasting were investigated in order to shed light on the soda-ash activation of boron within ludwigite ore, and to provide guidance for the extraction of boron from ludwigite ore. The conclusions were obtained as follows.

(1) Based on the thermodynamic calculation for the reaction between Na_2CO_3 and $MgSiO_3/Mg_2SiO_4$, the generation of Na_2MgSiO_4 was preferential in the temperature range 400−1400 °C, and the starting reaction temperatures are 707.57 °C and 855.93 °C, respectively. While, regarding the reaction between Na_2CO_3 and $Mg_2B_2O_5$, the formation of $NaBO_2$ was preferential and the starting reaction temperature was 1000 °C at CO_2 pressure of 1 atm.

(2) For the experimentally soda-ash roasting of lizardite or szaibelyite in nitrogen gas atmosphere, the reaction between sodium carbonate and the dehydroxylation products of lizardite ($MgSiO_3$ and Mg_2SiO_4) highly depended on the melting of sodium carbonate (melting point 851 °C), giving rise to the formation of Na_2MgSiO_4; while for the soda-ash roasting of szaibelyite, $NaBO_2$ was rapidly generated before the melting of sodium carbonate.

Author Contributions: Conceptualization and methodology, G.L., and M.R.; software, J.Y. and J.W.; investigation, X.Z., J.X., J.L., T.Z., and J.D.; writing X.Z., Z.P. and M.R.; funding acquisition, M.R. and T.J.

Funding: This research was funded by "the National Natural Science Foundation of China, grant number 51804346" and "the Hunan Provincial Natural Science Foundation of China, grant number 2019JJ50767".

Conflicts of Interest: The authors declare no conflict of interest.

References

1. An, J.; Xue, X. Life cycle environmental impact assessment of borax and boric acid production in China. *J. Clean. Prod.* **2014**, *66*, 121–127. [CrossRef]

2. Jiang, S.-Y.; Palmer, M.R.; Peng, Q.-M.; Yang, J.-H. Chemical and stable isotopic compositions of Proterozoic metamorphosed evaporites and associated tourmalines from the Houxianyu borate deposit, eastern Liaoning, China. *Chem. Geol.* **1997**, *135*, 189–211. [CrossRef]
3. Brioche, A.S. Mining Engineering—Research and Technology. In *Mineral Commodity Summaries 2019*; Nova Science Publishers: New York, NY, USA, 2019; 36p.
4. Palmer, M.R.; Helvaci, C. The boron isotope geochemistry of the Kirka borate deposit, western Turkey. *Geochim. Cosmochim. Acta* **1995**, *59*, 3599–3605. [CrossRef]
5. Peng, Q.M.; Palmer, M.R. The paleoproterozoic Mg and Mg-Fe borate deposits of Liaoning and Jilin Provinces, northeast China. *Econ. Geol. Bull. Soc. Econ. Geol.* **2002**, *97*, 93–108. [CrossRef]
6. Li, Y.-J.; Gao, T.; Han, Y.-X. Research on processing mineralogy of paigeite. *Non Ferr. Min. Metall.* **2006**, *22*, 3.
7. Liu, R.; Wang, X.J.; Gao, Y.L.; Lu, Q.; Xue, X.X. Reaction Synthesis and Oxidation Behaviours of Ludwigite. *Adv. Mater. Res.* **2011**, *146*, 6. [CrossRef]
8. Li, Z.H.; Han, Y.X.; Gao, P.; Ying, P. Research on Processing Mineralogical Characterization of the Paigeite Ore. *J. Northeast. Univ.* **2016**, *37*, 258–262.
9. Wang, G.; Xue, Q.; She, X.; Wang, J. Carbothermal Reduction of Boron-bearing Iron Concentrate and Melting Separation of the Reduced Pellet. *ISIJ Int.* **2015**, *55*, 751–757. [CrossRef]
10. Xu, Y.; Jiang, T.; Zhou, M.; Wen, J.; Chen, W.; Xue, X. Effects of mechanical activation on physicochemical properties and alkaline leaching of boron concentrate. *Hydrometallurgy* **2017**, *173*, 32–42. [CrossRef]
11. Wang, G.; Wang, J.; Ding, Y.; Ma, S.; Xue, Q. New Separation Method of Boron and Iron from Ludwigite Based on Carbon Bearing Pellet Reduction and Melting Technology. *ISIJ Int.* **2012**, *52*, 45–51. [CrossRef]
12. Duan, H.M.; Lü, X.; Ning, Z.; Zhai, Y. Boron extraction from boron-concentrate ore by ammonium sulfate roasting method. *J. Northeast. Univ.* **2011**, *32*, 1724–1728.
13. Liu, H.W.; Zhong, J.; Yu, T. Study on the technology of improving reactive activity of ludwigite from Wengquangou. *Inorg. Chem. Ind.* **2008**, *40*, 21–24.
14. Jiang, T.; Yin, L.; Zhu, L.; Xue, X.X. Preparation of borax from boron concentrate by sodium- roasting and leaching. *CIESC J.* **2014**, *65*, 737–743.
15. Li, G.; Liang, B.; Rao, M.; Zhang, Y.; Jiang, T. An innovative process for extracting boron and simultaneous recovering metallic iron from ludwigite ore. *Miner. Eng.* **2014**, *56*, 57–60. [CrossRef]
16. Qin, S.; Yin, B.; Zhang, Y.; Zhang, Y. Leaching kinetics of szaibelyite ore in NaOH solution. *Hydrometallurgy* **2015**, *157*, 333–339. [CrossRef]
17. Qin, S.; Zhang, Y.; Zhang, Y. Nucleation and morphology of sodium metaborate dihydrate from NaOH solution. *J. Cryst. Growth* **2016**, *433*, 143–147. [CrossRef]
18. Ning, Z.-Q.; Zhai, Y.-C.; Song, Q.-S. Extracting B_2O_3 from calcined boron mud using molten sodium hydroxide. *Rare Met.* **2015**, *34*, 744–751. [CrossRef]
19. Kim, J.W.; Lee, H.G. Thermal and carbothermic decomposition of Na_2CO_3 and Li(2)CO_3. *Metall. Mater. Trans. B Process Metall. Mater. Process. Sci.* **2001**, *32*, 17–24. [CrossRef]
20. Hu, B.S.; Xiong, F.W. The Influence of Serpentine Kind and Size on Sintering Process. *Sinter. Pelletizing* **2010**, *35*, 23–26.



© 2019 by the authors. Licensee MDPI, Basel, Switzerland. This article is an open access article distributed under the terms and conditions of the Creative Commons Attribution (CC BY) license (http://creativecommons.org/licenses/by/4.0/).